Geophysical Research Letters

RESEARCH LETTER
10.1029/2021GL095615

Key Points:

- The eastern Atlantic basin supports nearly 38 ± 14% of the southward North Atlantic deep water (NADW) transport in mid-latitudes
- The meridional transport of NADW in the eastern basin is due to the potential vorticity constraint imposed by the Mid-Atlantic Ridge

Supporting Information:

Supporting Information may be found in the online version of this article.

Correspondence to:

Y. Zhai and X. Wan,
yzhai@stu.ouc.edu.cn;
xqwan@ouc.edu.cn

Citation:

Zhai, Y., Yang, J., Wan, X., & Zou, S. (2021). The eastern Atlantic basin pathway for the export of the North Atlantic deep waters. *Geophysical Research Letters*, *48*, e2021GL095615. https://doi.org/10.1029/2021GL095615

Received 11 AUG 2021
Accepted 2 DEC 2021

The Eastern Atlantic Basin Pathway for the Export of the North Atlantic Deep Waters

Yujia Zhai[1,2], Jiayan Yang[2], Xiuquan Wan[1,3], and Sijia Zou[4]

[1]College of Oceanic and Atmospheric Sciences, Ocean University of China, Qingdao, China, [2]Department of Physical Oceanography, Woods Hole Oceanographic Institution, Woods Hole, MA, USA, [3]Physical Oceanography Laboratory/CIMST, Ocean University of China and Qingdao National Laboratory for Marine Science and Technology, Qingdao, China, [4]State Key Laboratory of Marine Environmental Science & College of Ocean and Earth Sciences, Xiamen University, Xiamen, China

Abstract The North Atlantic deep water (NADW), according to the classic ocean circulation theory, moves southward as a deep western boundary current (DWBC) even though it may veer into interior and then rejoin DWBC when encountering regional circulation features, such as eddy-driven recirculation. In potential vorticity dynamics, the eastern side of the Mid-Atlantic Ridge (MAR) may provide a similar topographic support as the continental slope off the western boundary for a southward transport of NADW. In this article, we quantify the mean meridional NADW transports on both sides of the MAR using a data-assimilated product and find that the flow in the eastern basin contributes about 38 ± 14% of the net southward transport of NADW from 50° to 35°N. Our study points to the importance of observing NADW transport variations on the eastern side of the MAR in order to monitor the transport strength of Atlantic Meridional Overturning Circulation.

Plain Language Summary Classic theory suggested that the Deep Western Boundary Current (DWBC) carries the cold and fresh North Atlantic deep water (NADW) from the high latitude to the south. However, float and tracer observations, albeit sparse, have revealed a possible southward pathway in the eastern North Atlantic, that is, east of the Mid-Atlantic Ridge (MAR). Using an ocean reanalysis product, the Estimating the Circulation and Climate of the Ocean (ECCOV4r4), we show that the steady-state NADW meridional transport in the basin east of the MAR accounts for about 38 ± 14% of the meridional transport in the whole basin between 35° and 50°N. It is found that the NADW circulation pathways are strongly influenced by ocean bottom topography. For example, the eastern flank of the MAR acts as a "western boundary" in the eastern basin against which NADW flows southward. The topographic constraint from the MAR weakens south of 35°N due to changes in the MAR height and smaller planetary vorticity f. The current study has improved our understanding of NADW transport structure at mid-latitude by quantifying the equatorward transport east of the MAR.

1. Introduction

The ocean influences the atmosphere primarily through the surface heat flux. The Atlantic Meridional Overturning Circulation (AMOC) is a leading mechanism for oceanic heat transport and thus an important component in the global climate system. The AMOC is driven in part by the formation and export of the North Atlantic deep water (NADW), which consists of three main components, that is, Labrador Sea Water (LSW), Denmark Strait Overflow Water (DSOW), and Iceland-Scotland Overflow Water (ISOW). The LSW is formed in the winter by deep convection in Labrador and Irminger Seas (Pickart et al., 2003; Talley & McCartney, 1982) and is lighter in density than the DSOW and ISOW. Originated from the Nordic Seas, DSOW and ISOW are subsequently diluted by mixing with ambient Atlantic Water at shelf break after the Nordic Seas source waters overflow the Greenland-Iceland-Scotland Ridge (Price & Baringer, 1994).

Talley and McCartney (1982) used observations to describe key features of LSW (low-salinity and low potential vorticity [PV]) and identify three main pathways for LSW in the subpolar North Atlantic Ocean, which are: (a) northeastward into the Irminger Sea; (b) southeastward across the Atlantic beneath the North Atlantic Current; and (c) southward past Newfoundland and then westward beneath the Gulf Stream. Later studies revealed a more complex pathway for the LSW spreading in the subpolar North Atlantic (e.g., Lavender et al., 2000; Paillet et al., 1998; Rhein et al., 2002; Yashayaev, 2007).

After entering the Iceland basin through the Iceland-Scotland ridge, ISOW flows southward along the eastern flank of the Reykjanes Ridge until it reaches the Charlie Gibbs Fracture Zone (CGFZ), where it moves westward to the western basin (Fleischmann et al., 2001; Smethie et al., 2000; Swift, 1984; van Aken, 2000). South of the CGFZ, observations revealed that a portion of ISOW continues southward along the eastern flank of the Mid-Atlantic Ridge (MAR) into the West European Basin (Fleischmann et al., 2001; Smethie et al., 2000).

As another important component of NADW, DSOW originated from the Nordic Seas, overflows the sill in the Denmark Strait and travels southward along the boundary in the western Irminger Basin (e.g., Dickson & Brown, 1994; Worthington, 1970). Observations have revealed the existence of DSOW as the densest component of DWBC (e.g., Schott et al., 2004; Toole et al., 2011).

The NADW exits the subpolar North Atlantic to spread to the global abyssal ocean. Stommel (1958) and Stommel and Aarons (1960a, 1960b) constructed the first dynamical model for an abyssal ocean circulation driven by the NADW formation. The main pathway for exporting the NADW, according to the Stommel-Arons model, is through the deep western boundary currents (DWBCs). Indeed, the existence of the DWBC in the North Atlantic Ocean was confirmed in observations (Warren, 1981). Later studies have provided more information about the mean and variability of DWBCs in the Atlantic Ocean (e.g., Fischer et al., 2010; Kanzow & Zenk, 2014; Toole et al., 2017).

However, Bower et al. (2009) found that the LSW is transported to the subtropical basin via interior pathways in addition to along the traditionally defined DWBC through analyzing the Range and Fixing of Sound (RAFOS) floats (Rossby et al., 1986) released from 2003 to 2005 in the upper NADW layer at 50°N. Floats left the DWBC preferentially at topographic choke points at the southeastern corner of the Flemish Cap and the Tail of the Grand Banks. Such interior pathways were also present in an eddy-resolving Ocean general circulation model (Gary et al., 2011). Lozier et al. (2013) further demonstrated the existence of interior pathways for the overflow waters from the Nordic Seas with historical hydrographic observations and model simulations which is similar to that of the LSW. Xu et al. (2015) also found the existence of interior pathway in their numerical simulations when analyzing the spreading of DSOW and they pointed out the importance of ocean bottom topography in guiding DSOW transport. These previous studies have focused primarily on NADW transport in the western North Atlantic, and possible pathways on the eastern side of the MAR remains underexplored. Studies based on tracers (Fleischmann et al., 2001) and Lagrangian floats (Biló & Johns, 2019; Gary et al., 2012; Zou et al., 2017) have described a potentially important southward pathway on the eastern side of the MAR. Fleischmann et al. (2001) estimated the deep water ($\sigma_\theta > 27.8 \mathrm{kg \cdot m^{-3}}$) transport (2.4–3.5 *Sv*, 1 $Sv = 10^6\ \mathrm{m^3\ s^{-1}}$) from the Iceland Basin to the West European Basin with observed tracer data. Biló and Johns (2019) assessed that the transport of LSW ($36.97\ \mathrm{kg \cdot m^{-3}} > \sigma_2 > 36.50\ \mathrm{kg \cdot m^{-3}}$) recirculates in the Newfoundland Basin is $9.3 \pm 3.5\ Sv$, while about $3.2 \pm 0.4\ Sv$ LSW transports east of the Azores at a quasi-zonal section with Argo data and the World Ocean Atlas product.

Topography plays a fundamental role in the dynamics of NADW transport. The abyssal ocean velocity is likely geostrophic because of its large spatial scales (relative to the internal deformation radius), weak velocity (small Rossby number) and insulation from a direct atmospheric forcing. Therefore, the abyssal flow is expected to be along the geostrophic contours. In a flat-bottom ocean model, like the Stommel-Arons model, the meridional flow is allowed along the western boundary where the frictional PV flux dominates or in the interior where the meridional advection of planetary vorticity is balanced by the vortex stretching due to upwelling. In a model with varying bathymetry, the geostrophic contours no longer need to be zonal and thus allow meridional flows even if there is no external forcing. For a WBC along a continental slope the frictional PV flux becomes important only when the cross-stream scale becomes comparable with the Munk layer width (Jackson et al., 2006). The MAR is the most prominent topographic feature that may disconnect geostrophic contours between the eastern and western sides of the ridge, and its meridional orientation provides a topographic support for a meridional flow in the eastern basin that could be dynamically similar to the DWBC on the continental slope off the western boundary. Like the DWBC, the friction becomes important only when the cross-stream of the flow becomes comparable with the width of frictional boundary layer.

Southward transport of the LSW on eastern side of the MAR has been identified in previous studies (e.g., Paillet et al., 1998). However, the transport is still not well quantified and the influence of the MAR on the transport pathways remains insufficiently studied. In this study, we use a data-assimilated product to quantify the mean

state meridional transport of NADW in both the eastern and western basins of the mid-latitude Atlantic. We also provide a mechanistic description about the influence of the MAR on NADW meridional transport distribution.

2. Data and Methods

2.1. Data: ECCOV4r4

In our analyses of the mean state of the AMOC lower limb, we use the ECCO4 release 4 (ECCOV4r4, ECCO Consortium et al., 2020, 2021; Forget et al., 2015) to obtain the full coverage of mid-latitude meridional transport. ECCOV4r4 is the latest release of ECCO version 4, covering a 26-yr period from 1992 to 2017. It is based on the MIT General Circulation Model (MITgcm) and assimilates most available modern oceanographic observations, including sea surface height from altimetry, ocean bottom pressure from the Gravity Recovery and Climate Experiment (GRACE), hydrography from Argo profilers, moorings, etc. (Fukumori et al., 2020). The estimate uses the adjoint method to improve fit to observations through repetitively minimizing the squared sum of weighted model-data misfits and control adjustments (Wang et al., 2020). We use the interpolated monthly product from https://www.ecco-group.org/products.htm. This gridded ECCOV4r4 data has a resolution of 0.5° horizontally and 50-levels vertically. One major appealing aspect of using ECCO4 is that it assimilates the ocean bottom pressure data from satellite observations and thus the geostrophic velocity in the abyssal ocean is better constrained toward a realistic state.

2.2. Methods: Definition of the Upper and Lower NADW Layers

To separate AMOC into the upper limb, which transports warm upper layer water northward, and the lower limb that returns cold NADW southward, we follow Lozier et al. (2019) by choosing ($\sigma_\theta = 27.66\ \mathrm{kg \cdot m^{-3}}$ as the interface between upper and lower limbs. Figure S1a in Supporting Information S1 shows the mean AMOC in density space and Figure S1b in Supporting Information S1 provides the maximum AMOC in density space. The mean maximum upper AMOC transport is about $15.4 \pm 1.8\ Sv$ (at 55°N), which is consistent with previous estimates at high latitude North Atlantic (e.g., Lozier et al., 2019). The difference between the maximum AMOC and upper limb AMOC (above $\sigma_\theta = 27.66\ \ kg \cdot m^{-3}$) is small as shown in Figure S1b in Supporting Information S1. Therefore, it appears that using ($\sigma_\theta = 27.66\ \mathrm{kg \cdot m^{-3}}$ as the boundary between the upper and lower AMOC limbs is appropriate in our analyses of ECCOV4r4. In addition, we also compare AMOC transport in ECCOV4r4 with two long-time AMOC transport observations (see Text S1 and Table T1 in Supporting Information S1) at low latitude Atlantic. The results show that the AMOC transport in ECCOV4r4 is slightly weaker than observed transport.

In this study, the NADW is separated into two layers: one is the upper NADW layer which primarily consists of LSW, and the other is the lower NADW layer which lays under the upper NADW layer and includes both DSOW and ISOW. Following previous studies, the potential density surface ($\sigma_\theta = 27.8\ \mathrm{kg \cdot m^{-3}}$ is selected to separate the upper and lower NADW layers (e.g., Gary et al., 2012; Pickart & Spall, 2007; Sarafanov et al., 2012; Saunders, 1994; Stramma et al., 2004). Figure 1a shows the bathymetry of North Atlantic in ECCOV4r4 and the locations of five sections, both zonal and meridional, along which the salinity (color) potential density (contour lines) are shown (Figures 1b–1f). The low salinity water that is characteristic of LSW is present on both sides of the MAR in the intermediate depth as Figures 1b and 1e shown.

Taking a consideration of the complex nature of the bathymetry, we define two meridional sections on two sides of the MAR that are parallel to the ridge (Figures 1d and 1f). As expected, the upper layer with a high salinity is thick in the subtropical basin, reaching the maximum thickness near 37°N as shown in Figures 1e and 1f. In addition, the salinity along the zonal section at 40°N (Figure 1c) clearly shows the water mass is saltier in the eastern Atlantic, which is resulted from the presence of the high salinity Mediterranean Outflow Water (MOW) and the eastward shift of the North Atlantic Current at that latitude (e.g., Baringer & Price, 1997; Iorga & Lozier, 1999). The salinity of 36.25 has been used in some studies to characterize the MOW (e.g., Baringer & Price, 1997; Iorga & Lozier, 1999), while Ferreira and Kerr (2017) used salinity 35.5 to mark Mediterranean Water. In our study, we calculate the meridional transport of NADW by excluding water masses with salinity >35.5. Additionally, to separate the NADW from the Antarctic Bottom Water (AABW) in the deep North Atlantic, we choose ($\sigma_4 = 45.91\mathrm{kg\ m^{-3}}$ as the top boundary of AABW (as shown in Figures 1c, 1d and 1f), consistent with previous studies (e.g., Talley, 2008).

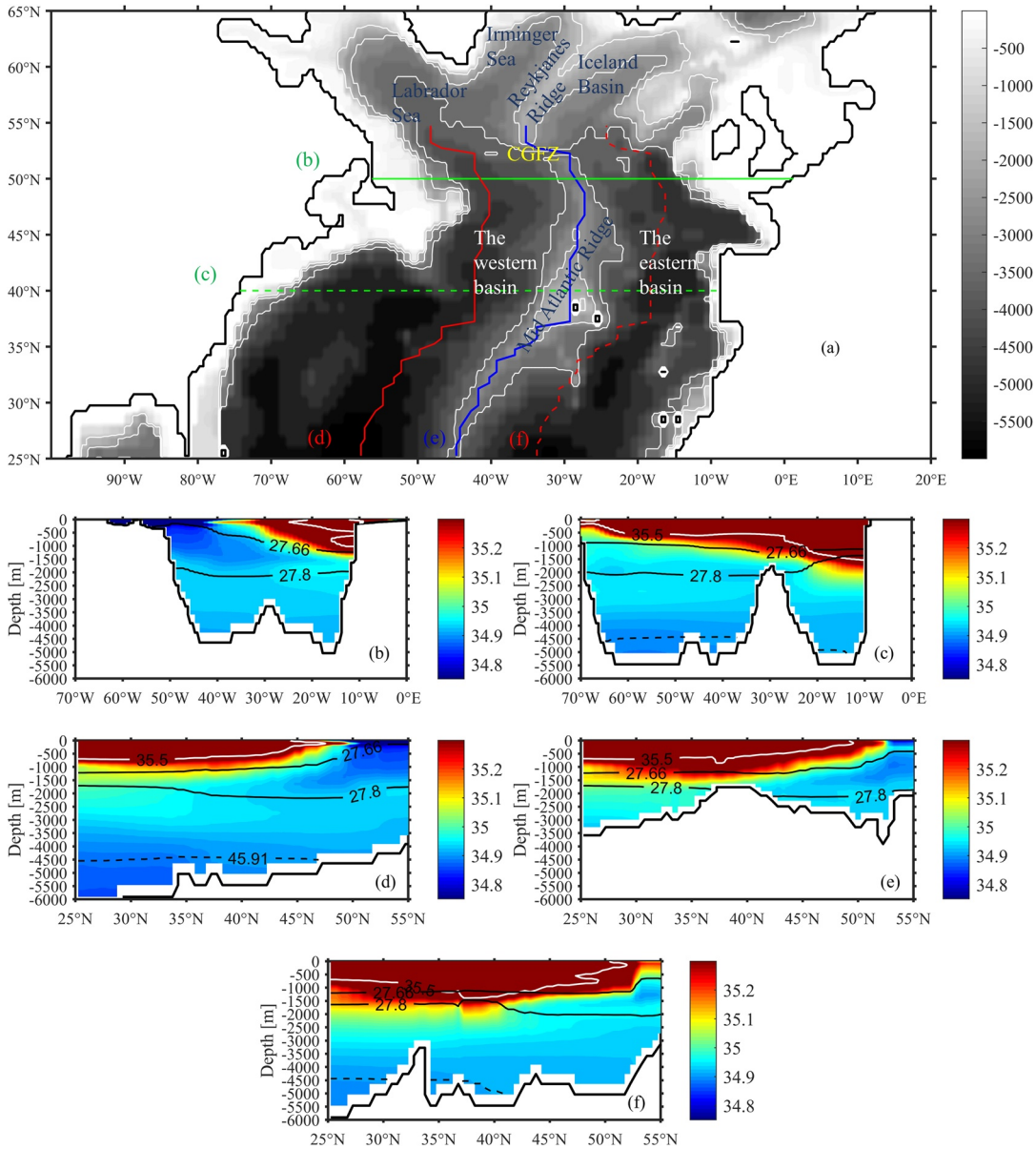

Figure 1. (a) The bathymetry (m) used in ECCOV4r4 in color. Colored solid lines make sections along which the salinity (color) and potential density (lines) are shown in (b–f). Green solid line for a zonal section at 50°N for (b), and green dashed line for 40°N for (c), blue line along the MAR for (e), solid red line for a meridional section about 13° to the west of MAR section for (d), and dashed red line for a meridional section 11° to the east of MAR section for (f). The gray contours are for 1,500, 2,500, and 3,500 m isobaths. (b–f) The white contours mark $S = 35.5$ in salinity, the black solid contours show the potential density ($\sigma_\theta = 27.66$ and 27.8 kg · m^{-3}, and the black dashed line contours are the potential density ($\sigma_4 = 45.91$ kg · m^{-3}).

3. Results

3.1. Meridional Transport of NADW

Figure 2 shows the latitudinal distribution of the meridional transports in the upper and lower NADW layers, respectively (see details in Text S2 in Supporting Information S1). The calculation of meridional transport does not include MOW (salinity > 35.5), which makes a relatively small contribution to the meridional transport both in the upper and lower NADW layers (as shown in Figures S2a–S2f in Supporting Information S1). The calculation of the lower NADW layer follows the same procedure except for a different density range (between $\sigma_\theta = 27.8$ kg · m^{-3} and $\sigma_4 = 45.91$ kg · m^{-3}) without an AABW component. The magnitude of AABW transport shown in Figures S2g–S2i in Supporting Information S1 is small compared with the NADW transport. In the

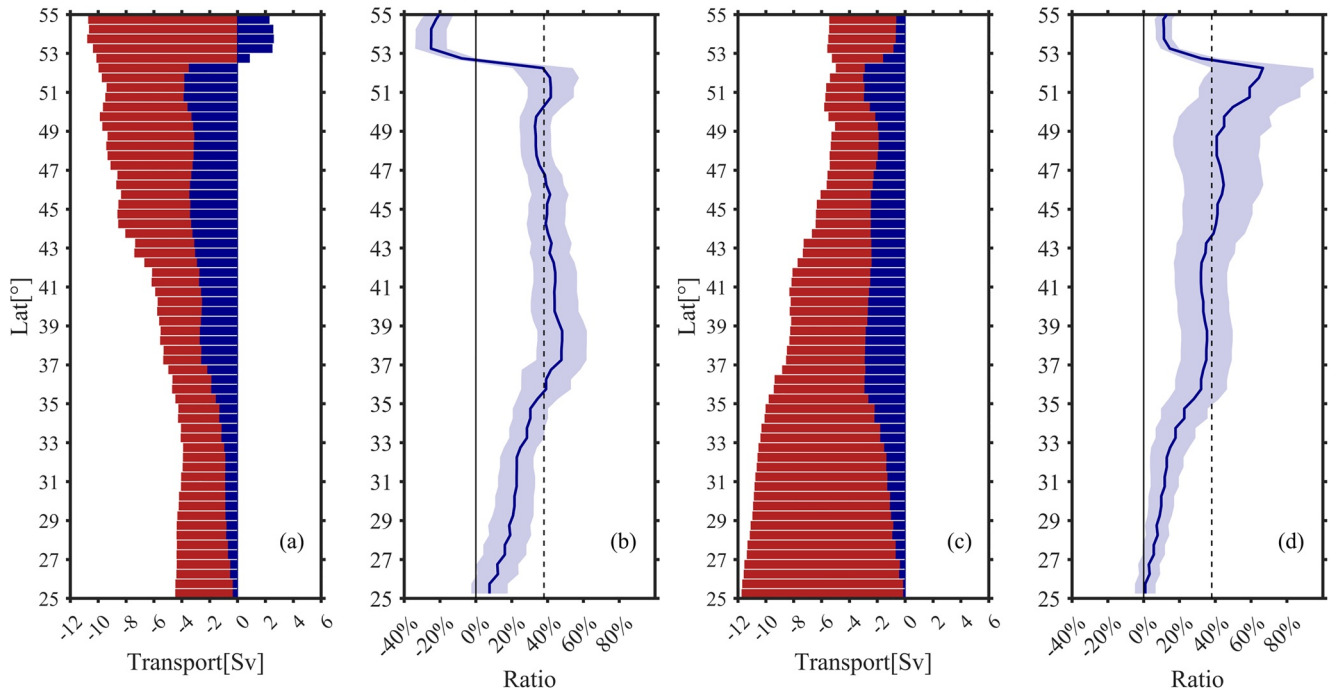

Figure 2. (a) The net meridional transport [Sv] in the upper NADW layer from ECCOV4r4 across the whole basin ($T_w + T_e$) (red bars), and the transport component in the eastern basin (T_e) (blue bars); (b) The percentage of the eastern basin component in the upper NADW layer transport as defined by ($T_e/(T_w + T_e)$); (T_w is the upper NADW layer meridional transport in the western basin and defined as $T_w(y) = \int_{x=western\ \ boundary}^{x=MAR} \int_{\sigma_\theta=27.8\ \ kg\cdot m^{-3}}^{z_{\sigma_\theta=27.66\ \ kg\cdot m^{-3}}} v(x,y,z)dzdx$; T_e is the upper NADW layer meridional transport in the eastern basin and defined as $T_e(y) = \int_{x=MAR}^{x=eastern\ \ boundary} \int_{z_{\sigma_\theta=27.8\ \ kg\cdot m^{-3}}}^{z_{\sigma_\theta=27.66\ \ kg\cdot m^{-3}}} v(x,y,z)dzdx$. x = MAR is the crest position of the MAR indicated by the blue line in Figure 1(a). (c) and (d) are same as (a) and (b) except for the lower NADW layer. The black dashed lines indicate 38%. The standard deviation is marked with the light blue shadow zones in (b) and (d), separately.

eastern basin the meridional transport in the upper NADW layer diverges at the latitude of CGFZ, which is about 52°N, that is, northward (southward) to the north (south) of this latitude. Previous studies revealed an eastward transport of LSW through CGFZ (e.g., Talley & McCartney, 1982). Once into the eastern basin, some spreads northeastward to the eastern Iceland Basin (Rhein et al., 2002), and some flows southward along the eastern flank of the MAR (Paillet et al., 1998). The bifurcation of the meridional transport direction in the eastern basin in the upper NADW layer is consistent with the LSW spreading pathway. In addition, we also calculate the average of meridional NADW transport (combining the upper and lower NADW layer) between 35° and 50°N. The NADW transport over the whole basin is -14.3 ± 1.4 Sv (-7.1 ± 0.9 Sv in the upper NADW layer and -7.2 ± 1.6 Sv in the lower NADW layer), while the transport component in the eastern basin is -5.3 ± 1.7 Sv (-2.8 ± 0.8 Sv in the upper NADW layer and -2.5 ± 1.1 Sv in the lower NADW layer). Then, we calculate the percentage of eastern basin transport with the annual mean time series of the latitude-averaged NADW transport (between 35° and 50°N). As shown in Figures 2b and 2d, the meridional NADW transport east of the MAR accounts for nearly $38 \pm 14\%$ of the whole basin meridional NADW transport at mid-latitude.

In addition, the meridional transport decreases (increases) in the upper (lower) NADW layer while approaching lower latitudes. South of 35°N, the meridional transport in the eastern basin decreases and converges to the western basin in both the upper and lower NADW layers. In order to understand the circulation in the upper and lower NADW layers, we analyze the layer depth-averaged velocities and layer PV in the next section.

3.2. Layer Analyses

To better understand the transport pathways in the upper NADW layer, we calculate the thickness of the upper NADW layer and the depth-averaged velocities. Figure 3a shows that the area with large layer thickness locates near the exit of Labrador Sea where newly formed LSW is exported. A tongue extends eastward near 52°N to the fracture zone in the MAR, the location of CGFZ. Near the eastern boundary south of 52°N, the shrinking of the

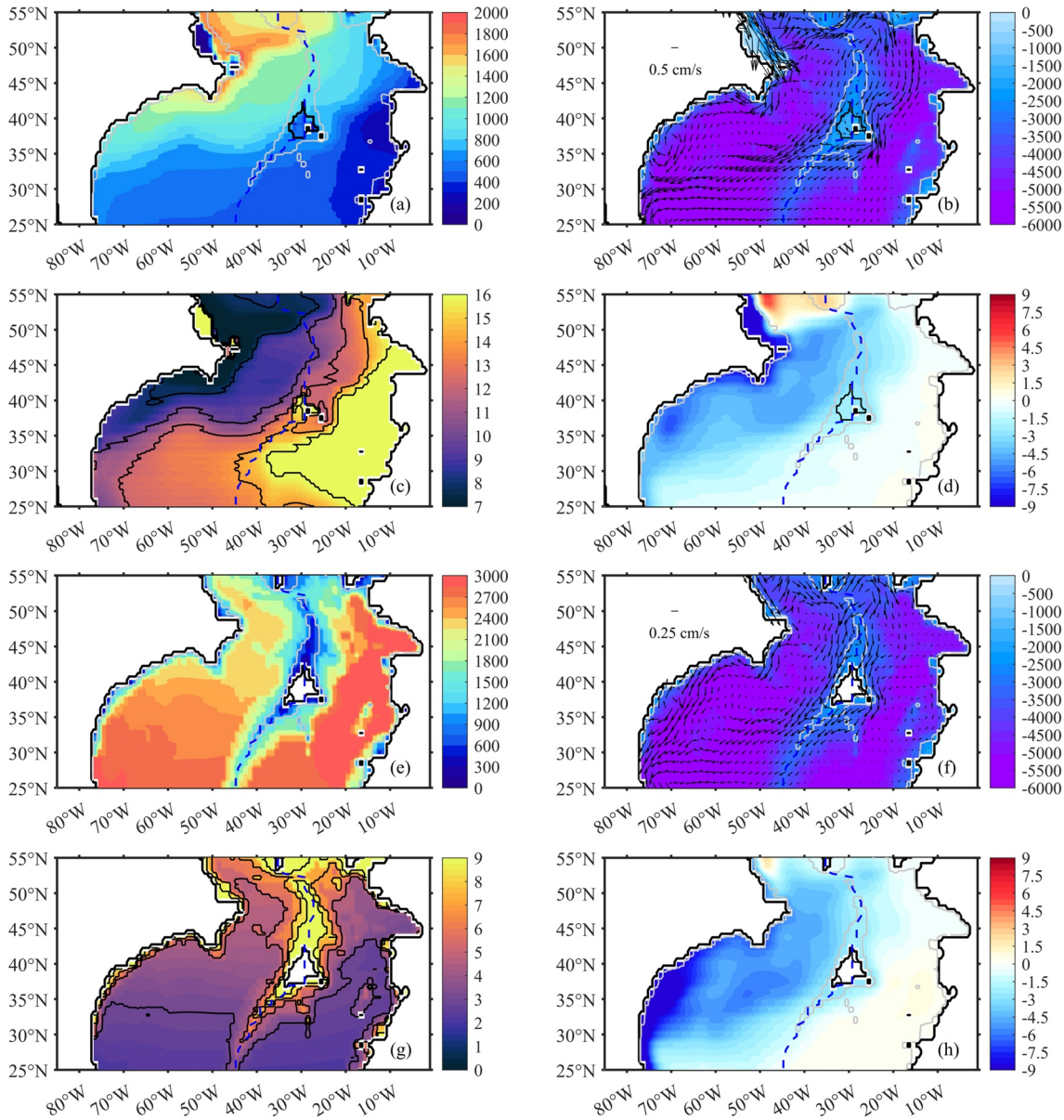

Figure 3. (a) Mean thickness (m) of the upper NADW layer ($\sigma_\theta = 27.66 - 27.8\ \ kg \cdot m^{-3}$); (b) mean depth-averaged circulation (cm/s) in the upper NADW layer (for the purpose of a better illustration, the depth-averaged velocities are truncated at 1.5 cm/s; the standard deviation of the depth-averaged circulation is shown in Figure S3 in Supporting Information S1; the calculation method is illustrated with Text S3 in Supporting Information S1); (c) the layer PV f/h [$10^{-8}\ \ m^{-1}s^{-1}$] in the upper NADW layer where h is defined as the layer thickness (for the purpose of a better illustration, the layer PV are truncated at $1.6 \times 10^{-7}\ \ m^{-1}s^{-1}$); (d) mean transport stream function (Sv) in the upper NADW layer, which is defined as $\varphi(x, y) = \int_{x=eastern\ \ boundary}^{x} \int_{z_{27.8\ \ kg\cdot m^{-3}}}^{z_{27.66\ \ kg\cdot m^{-3}}} v(x, y, z) dz dx$ (positive for northward transport). The blue dashed lines mark the location of the MAR. The gray contours are isobaths for 3000 m. The black contours in (a), (b) and (d) marks the area that bottom topography of the MAR intersects the upper NADW layer. The black contours in (c) are the layer PV contours. (e)–(h) are same as (a)–(d) except for the lower NADW layer. For the purpose of a better illustration, the depth-averaged velocities are truncated at 0.3 cm/s in (f) and the layer PV are truncated at $9 \times 10^{-8}\ \ m^{-1}s^{-1}$ in (g).

layer thickness might result from mixing with the overlying waters, the saline MOW (e.g., Iorga & Lozier, 1999; Talley & McCartney, 1982). Additionally, the thickness of the upper NADW layer decreases equatorward, which is consistent with the latitudinal changes of meridional transport (shown in Figure 2a).

Figure 3b illustrates the depth-averaged circulation in the upper NADW layer. The DWBC along the continental slope off the western boundary is a prominent feature, consistent with the classic view that it is a main conduit for the southward export of the NADW. Interestingly, the southward transport is strong along the MAR between 35° and 50°N especially on the eastern side of the MAR. However, the transport moves westward over the ridge and

converges toward the DWBC between 30° and 35°N. This diminished contribution from the eastern basin to the net basin-wide transport of the upper NADW south of 35°N is also evident in Figures 2a and 2b.

The interior flow away from boundary currents is likely to be predominantly geostrophic and, therefore, expected to follow the isolines of planetary PV, that is, f/h, where h is the layer thickness of upper NADW in the present case. Indeed, the velocity in the upper NADW layer, shown in Figure 3b, is mostly along PV contours (Figure 3c), such as the significant eastward transport near 52°N and the southwestward flow over the ridge toward the western basin south of 35°N. Obviously, the steady interior mid-latitude meridional transport in the upper NADW layer is strongly constrained by the layer PV distribution.

Previous studies about the LSW interior pathway also revealed similar flow structure in the eastern basin (e.g., Biló & Johns, 2019; Gray et al., 2012). It is interesting to note that the flow in the upper NADW layer is influenced by bathymetric features associated with the MAR even though this layer of water mass is mostly above the seafloor except in a few isolated regions where the layer intersects with the ridge (black contours in Figure 3d). The dynamics of how topography can exert a considerable influence on a stratified geostrophic flow above the bottom layer is explained in an idealized model by Brink (1998, 2016). The influence is facilitated by the continuity of the vertical velocity in a geostrophic flow, which is horizontally nondivergent. Such a bathymetric effect is particularly strong when the lateral scale of bathymetry variation is smaller than f/β—an assumption that is mostly valid for the present case of a mid-latitude flow over a ridge with a cross-ridge scale of a few hundred kilometers. The westward convergence over the ridge from the eastern basin toward the DWBC at 35°N is mainly due to the lessened topographic effects on f/h contours when the crest of the ridge becomes deeper (and thus less topographic constraint) and the planetary vorticity f becomes smaller when the water moves closer to the equator.

Comparing with the upper NADW layer shown in Figure 3a, the thickness of the lower NADW layer (Figure 3e) increases toward lower latitudes both in the western and eastern basins, which is consistent with the meridional transport latitudinal changes shown in Figure 2c. It is noted here that the net NADW transport, combining the upper and lower layers, remains relatively steady at about $-14.8 \pm 1.3\ Sv$ across latitudes (from 25° to 55°N), as shown in Figure 2. The decline of the upper NADW transport toward lower latitudes is compensated by an increase of similar magnitude in the lower NADW transport. Our analyses indicate that the transport partition between these two components is sensitive to the choice of potential density for their interface ($\sigma_\theta = 27.8$ $\mathrm{kg \cdot m^{-3}}$ in our analyses). The compensating changes between transports in these two NADW layers are likely due to diapycnal mixing in the model. Observations have revealed that the mixing between LSW and MOW happens when LSW spreads toward lower latitudes (e.g., Talley & McCartney, 1982). Figures 2b and 2d show that the percentage of the net southward transport occurs in the eastern basin in both layers is close to $38 \pm 14\%$ which is calculated by combining the latitude-averaged transport between 35° and 50°N in upper and lower NADW layers. Therefore, the main conclusion remains valid that the transport in the eastern basin makes an important, albeit smaller, contribution to the net southward transport of the NADW.

Figure 3f depicts that the lower NADW flows southward both in the western and eastern flanks of the MAR. The southward flow in the eastern basin between 35° and 50°N is mainly along the MAR eastern slope where the bathymetry, like the continental slope in the western basin, makes the geostrophic contours to be meridionally oriented. There is also a southward flow on the western flank of the MAR which might be attributed to the similar dynamical constraint discussed by Yang and Pratt (2014) for deep-water flow around Iceland-Faroe Ridge. South of 35°N, most of the southward flow in the eastern basin turns southwestward into the western basin, while a fraction continues to flow along the eastern flank of MAR. The crest of the MAR deepens south of 35°N (shown in Figure 1a), which, together with a decreasing value of planetary vorticity f, helps to alleviate the topographic constraint imposed by the ridge and allow the geostrophic contours to be extended zonally across the MAR. This relaxation of the topographic constraint is similar to what happens in the upper NADW layer discussed above.

There is an eastward flow through the CGFZ in the lower NADW layer that seems to be in disagreement with previous studies that show a westward mean flow through the CGFZ (Bower & Furey, 2017), even though occasionally eastward flow was observed in the fracture zone due to deep reaching North Atlantic Current (Schott et al., 1999). As shown in Figure S4 in Supporting Information S1, in the lower NADW layer, the westward and eastward zonal velocities coexist in the mean state from ECCOV4r4. Additionally, the estimated ISOW transport in the Iceland Basin from ECCOV4r4 (not shown) is about $-0.6 \pm 0.2\ Sv$, which is weaker than the observation-based estimate of $-3.8 \pm 0.6\ Sv$ (Kanzow & Zenk, 2014). The discrepancy for ISOW between observations

and ECCOV4r4 might be resulted from the coarse resolution and the underrepresentation of the overflows due to parameterization issues in the ECCO model, as well as insufficient observations in abyssal ocean to constrain the model.

It is worth noting that our results are based on product of state estimate and will need to be validated by observations. We did repeat the same analyses using a different state estimate, the Global Seasonal forecast system version 5 (Glosea5), which is a high-resolution reanalysis product based on the Nucleus for European Modelling of the Ocean (NEMO) model (Blockley et al., 2014; MacLachlan et al., 2015). The results (not shown) are qualitatively similar to that shown in Figure 2 that the transport of the upper and lower NADW on the eastern side of the MAR accounts for about 30%–50% of the total transport between 35° and 50°N.

4. Summary

In this study, we describe and analyze the meridional transport of NADW distribution both in the upper and lower layers in the mid-latitude North Atlantic Ocean with a data-assimilated product ECCOV4r4. The NADW flows southward in the basins both east and west of the MAR. Between 35° and 50°N, the southward transport in the eastern basin consists of nearly $38 \pm 14\%$ of the whole basin meridional transport both in the upper and lower NADW layers. At this latitude band, the net mean meridional transport across the whole basin is $-7.1 \pm 0.9\ Sv$ ($-7.2 \pm 1.6\ Sv$) in the upper (lower) NADW layer, while the eastern basin meridional transport is $-2.8 \pm 0.8\ \ Sv$ ($-2.5 \pm 1.1\ \ Sv$). The existence of the eastern basin pathways is mainly attributable to the MAR. The convergence of the transport toward the DWBCs at about 35°N follows the PV contours that extend across the ridge due to the deeper crest and smaller planetary vorticity f. Our results indicate that the southward transport of the NADW to the east of the MAR makes an important contribution to the lower limb of AMOC and suggest that its variability needs to be monitored in order to quantify the net transport variability in the NADW layer.

Data Availability Statement

The ECCOV4r4 products can be accessed at https://ecco.jpl.nasa.gov/drive/files/Version4/Release4/interp_monthly. The RAPID data are freely available from https://rapid.ac.uk/rapidmoc/rapid_data/datadl.php. The MOVE data are freely available from http://mooring.ucsd.edu/index.html?/projects/move/move_intro.html. The Glosea5 data are downloaded from https://resources.marine.copernicus.eu/product-detail/GLOBAL_REANALYSIS_PHY_001_031/INFORMATION.

Acknowledgments
Jiayan Yang is supported by the WHOI-OUC Collaborative Initiative, the W. V. A. Clark Chair for Excellence in Oceanography from WHOI, and National Science Foundation. Sijia Zou acknowledges the support from the Physical Oceanography Program of the United States National Science Foundation Grants OCE-1756361. Yujia Zhai is supported by China Scholarship Council as a 2-yr guest student to visit WHOI. Yujia Zhai and Xiuquan Wan are supported by major project (41776009) of National Natural Science Foundation of China. Data from the RAPID MOC monitoring project are funded by the Natural Environment Research Council and are freely available from www.rapid.ac.uk/rapidmoc. Collection of MOVE data was funded by NOAA Research, and carried out by principal investigators Uwe Send and Matthias Lankhorst. MOVE data are made freely available through the international OceanSITES program. We sincerely thank the two reviewers for their constructive and thoughtful comments that have helped us improve our work.

References

Baringer, M. O., & Price, J. F. (1997). Mixing and spreading of the mediterranean outflow. *Journal of Physical Oceanography*, *27*(8), 1654–1677. https://doi.org/10.1175/1520-0485(1997)027<1654:MASOTM>2.0.CO;2

Biló, T. C., & Johns, W. E. (2019). Interior pathways of Labrador Sea water in the North Atlantic from the Argo perspective. *Geophysical Research Letters*, *46*, 3340–3348. https://doi.org/10.1029/2018GL081439

Blockley, E. W., Martin, M. J., McLaren, A. J., Ryan, A. G., Waters, J., Lea, D. J., et al. (2014). Recent development of the Met Office operational ocean forecasting system: An overview and assessment of the new global FOAM forecasts. *Geoscientific Model Development*, *7*, 2613–2638. https://doi.org/10.5194/gmd-7-2613-2014

Bower, A., & Furey, H. (2017). Iceland-Scotland overflow water transport variability through the Charlie-Gibbs fracture zone and the impact of the North Atlantic current. *Journal of Geophysical Research*, *122*, 6989–7012. https://doi.org/10.1002/2017JC012698

Bower, A., Lozier, M., Gary, S., & Böning, C. (2009). Interior pathways of the North Atlantic Meridional Overturning Circulation. *Nature*, *459*, 243–247. https://doi.org/10.1038/nature07979

Brink, K. H. (1998). Deep-sea forcing and exchange processes. In K. H. Brink & A. R. Robinson (Eds.), *The sea* (pp. 63–88). John Wiley.

Brink, K. H. (2016). Cross-shelf exchange. *Annual Review of Marine Science*, *8*, 59–78. https://doi.org/10.1146/annurev-marine-010814-015717

Dickson, R. R., & Brown, J. (1994). The production of North Atlantic deep water: Sources, rates, and pathways. *Journal of Geophysical Research*, *99*(C6), 12319–12341. https://doi.org/10.1029/94JC00530

ECCO Consortium, Fukumori, I., Wang, O., Fenty, I., Forget, G., Heimbach, P., & Ponte, R. M. (2020). *ECCO central estimate (version 4 release 4)*. Retrieved from https://ecco.jpl.nasa.gov/drive/files/Version4/Release4/interp_monthly

ECCO Consortium, Fukumori, I., Wang, O., Fenty, I., Forget, G., Heimbach, P., & Ponte, R. M. (2021). *Synopsis of the ECCO central production global ocean and sea-ice state estimate (version 4 release 4)*. Zenodo. https://doi.org/10.5281/zenodo.4533349

Ferreira, M. L., & Kerr, R. (2017). Source water distribution and quantification of North Atlantic deep water and Antarctic bottom water in the Atlantic Ocean. *Progress in Oceanography*, *153*, 66–83. https://doi.org/10.1016/j.pocean.2017.04.003

Fischer, J., Visbeck, M., Zantopp, R., & Nunes, N. (2010). Interannual to decadal variability of outflow from the Labrador Sea. *Geophysical Research Letters*, *37*, L24610. https://doi.org/10.1029/2010GL045321

Fleischmann, U., Hidebrandt, H., Putzka, A., & Bayer, R. (2001). Transport of newly ventilated deep water from the Iceland Basin to the Westeuropean Basin. *Deep Sea Research Part I: Oceanographic Research Papers*, *48*(8), 1793–1819. https://doi.org/10.1016/S0967-0637(00)00107-2

Forget, G., Campin, J.-M., Heimbach, P., Hill, C. N., Ponte, R. M., & Wunsch, C. (2015). ECCO version 4: An integrated framework for non-linear inverse modeling and global ocean state estimation. *Geoscientific Model Development*, *8*, 3071–3104. https://doi.org/10.5194/gmd-8-3071-2015

Fukumori, I., Wang, O., Fenty, I., Forget, G., Heimbach, P., & Ponte, R. M. (2020). *ECCO version 4 release 4*. Retrieved from https://ecco.jpl.nasa.gov/drive/files/Version4/Release4/doc/v4r4_synopsis.pdf

Gary, S. F., Lozier, M. S., Biastoch, A., & Böning, C. W. (2012). Reconciling tracer and float observations of the export pathways of Labrador Sea Water. *Geophysical Research Letters*, *39*, L24606. https://doi.org/10.1029/2012GL053978

Gary, S. F., Lozier, M. S., Böning, C. W., & Biastoch, A. (2011). Deciphering the pathways for the deep limb of the meridional overturning circulation. *Deep Sea Research Part II: Topical Studies in Oceanography*, *58*(17–18), 1781–1797. https://doi.org/10.1016/j.dsr2.2010.10.059

Iorga, M. C., & Lozier, M. S. (1999). Signatures of the Mediterranean outflow from a North Atlantic climatology: 1. Salinity and density fields. *Journal of Geophysical Research*, *104*(C11), 25985–26009. https://doi.org/10.1029/1999JC900115

Jackson, L., Hughes, C., & Williams, R. (2006). Topographic control of basin and channel flows: The role of bottom pressure torques and friction. *Journal of Physical Oceanography*, *36*, 1786–1805. https://doi.org/10.1175/JPO2936.1

Kanzow, T., & Zenk, W. (2014). Structure and transport of the Iceland Scotland overflow plume along the Reykjanes Ridge in the Iceland basin. *Deep Sea Research Part I: Oceanographic Research Papers*, *86*, 82–93. https://doi.org/10.1016/j.dsr.2013.11.003

Lavender, K., Davis, R., & Owens, W. (2000). Mid-depth recirculation observed in the interior Labrador and Irminger seas by direct velocity measurements. *Nature*, *407*, 66–69. https://doi.org/10.1038/35024048

Lozier, M. S., Gary, S. F., & Bower, A. S. (2013). Simulated pathways of the overflow waters in the North Atlantic: Subpolar to subtropical export. *Deep Sea Research Part II: Topical Studies in Oceanography*, *85*, 147–153. https://doi.org/10.1016/j.dsr2.2012.07.037

Lozier, M. S., Li, F., Bacon, S., Bahr, F., Bower, A. S., Cunningham, S. A., et al. (2019). A sea change in our view of overturning in the subpolar North Atlantic. *Science*, *363*, 516–521. https://doi.org/10.1126/science.aau6592

MacLachlan, C., Arribas, A., Peterson, K. A., Maidens, A., Fereday, D., Scaife, A. A., et al. (2015). Global Seasonal forecast system version 5 (GloSea5): A high-resolution seasonal forecast system. *Quarterly Journal of the Royal Meteorological Society*, *141*, 1072–1084. https://doi.org/10.1002/qj.2396

Paillet, J., Arhan, M., & McCartney, M. S. (1998). Spreading of Labrador Sea water in the eastern North Atlantic. *Journal of Geophysical Research*, *103*(C5), 10223–10239. https://doi.org/10.1029/98jc00262

Pickart, R. S., & Spall, M. A. (2007). Impact of Labrador Sea convection on the North Atlantic meridional overturning circulation. *Journal of Physical Oceanography*, *37*(9), 2207–2227. https://doi.org/10.1175/JPO3178.1

Pickart, R. S., Straneo, F., & Moore, G. W. K. (2003). Is Labrador Sea water formed in the Irminger Basin? *Deep Sea Research Part I: Oceanographic Research Papers*, *50*(1), 23–52. https://doi.org/10.1016/S0967-0637(02)00134-6

Price, J. F., & Baringer, M. O. (1994). Outflows and deep water production by marginal seas. *Progress in Oceanography*, *33*(3), 161–200. https://doi.org/10.1016/0079-6611(94)90027-2

Rhein, M., Fischer, J., Smethie, W. M., Smythe-Wright, D., Weiss, R. F., Mertens, C., et al. (2002). Labrador Sea water: Pathways, CFC inventory, and formation rates. *Journal of Physical Oceanography*, *32*(2), 648–665. https://doi.org/10.1175/1520-0485(2002)032<0648:lswpci>2.0.co;2

Rossby, H. T., Dorson, D., & Fontaine, J. (1986). The RAFOS system. *Journal of Atmospheric and Oceanic Technology*, *3*(4), 672–679. https://doi.org/10.1175/1520-0426(1986)003<0672:trs>2.0.co;2

Sarafanov, A., Falina, A., Mercier, H., Sokov, A., Lherminier, P., Gourcuff, C., et al. (2012). Mean full-depth summer circulation and transports at the northern periphery of the Atlantic Ocean in the 2000s. *Journal of Geophysical Research*, *117*, C01014. https://doi.org/10.1029/2011JC007572

Saunders, P. M. (1994). The flux of overflow water through the Charlie-Gibbs Fracture Zone. *Journal of Geophysical Research*, *99*(C6), 12343–12355. https://doi.org/10.1029/94JC00527

Schott, F. A., Stramma, L., & Fischer, J. (1999). Interaction of the North Atlantic current with the deep Charlie Gibbs fracture zone throughflow. *Geophysical Research Letters*, *26*(3), 369–372. https://doi.org/10.1029/1998GL900223

Schott, F. A., Zantopp, R., Stramma, L., Dengler, M., Fischer, J., & Wibaux, M. (2004). Circulation and dDeep-wWater eExport at the wWestern eExit of the sSubpolar North Atlantic. *Journal of Physical Oceanography*, *34*(4), 817–843. https://doi.org/10.1175/1520-0485(2004)034<0817:CADEAT>2.0.CO;2

Smethie, W. M., Fine, R. A., Putzka, A., & Jones, E. P. (2000). Tracing the flow of North Atlantic deep water using chlorofluorocarbons. *Journal of Geophysical Research*, *105*(C6), 14297–14323. https://doi.org/10.1029/1999JC900274

Stommel, H. (1958). The abyssal circulation. *Deep Sea Research (Letters)*, *5*, 80–82. https://doi.org/10.1016/S0146-6291(58)80014-4

Stommel, H., & Arons, A. B. (1960a). On the abyssal circulation of the world ocean. I. Stationary planetary flow patterns on a sphere. *Deep Sea Research*, *6*, 140–154. https://doi.org/10.1016/0146-6313(59)90065-6

Stommel, H., & Arons, A. B. (1960b). On the abyssal circulation of the world ocean. II. An idealized model of the circulation pattern and amplitude in oceanic basins. *Deep Sea Research*, *6*, 217–233. https://doi.org/10.1016/0146-6313(59)90075-9

Stramma, L., Kieke, D., Rhein, M., Schott, F., Yashayaev, I., & Koltermann, K. P. (2004). Deep water changes at the western boundary of the subpolar North Atlantic during 1996 to 2001. *Deep Sea Research Part I: Oceanographic Research Papers*, *51*(8), 1033–1056. https://doi.org/10.1016/j.dsr.2004.04.001

Swift, J. H. (1984). The circulation of the Denmark Strait and Iceland-Scotland overflow waters in the North Atlantic. *Deep Sea Research Part A. Oceanographic Research Papers*, *31*(11), 1339–1355. https://doi.org/10.1016/0198-0149(84)90005-0

Talley, L. D. (2008). Freshwater transport estimates and the global overturning circulation: Shallow deep and throughflow components. *Progress in Oceanography*, *78*(4), 257–303. https://doi.org/10.1016/j.pocean.2008.05.001

Talley, L. D., & McCartney, M. S. (1982). Distribution and circulation of Labrador Sea water. *Journal of Physical Oceanography*, *12*(11), 1189–1205. https://doi.org/10.1175/1520-0485(1982)012<1189:DACOLS>2.0.CO;2

Toole, J. M., Andres, M., Le Bras, I. A., Joyce, T. M., & McCartney, M. S. (2017). Moored observations of the deep western boundary current in the NW Atlantic: 2004–2014. *Journal of Geophysical Research: Oceans*, *122*, 7488–7505. https://doi.org/10.1002/2017JC012984

Toole, J. M., Curry, R. G., Joyce, T. M., McCartney, M., & Peña-Molino, B. (2011). Transport of the North Atlantic deep western boundary current about 39°N, 70°W: 2004–2008. *Deep Sea Research Part II: Topical Studies in Oceanography*, *58*(17–18), 1768–1780. https://doi.org/10.1016/j.dsr2.2010.10.058

van Aken, H. (2000). The hydrography of the mid-latitude northeast Atlantic Ocean I: The deep water masses. *Deep Sea Research Part I: Oceanographic Research Papers*, *47*(5), 757–788. https://doi.org/10.1016/S0967-0637(99)00092-8

Wang, O., Fukumori, I., & Fenty, I. (2020). *ECCO version 4 release 4 user guide*. Retrieved from https://ecco.jpl.nasa.gov/drive/files/Version4/Release4/doc/v4r4_user_guide.pdf

Warren, B. A. (1981). Deep circulation of the world ocean. In B. A. Warren & C. Wunsch (Eds.), *Evolution of physical oceanography* (pp. 6–41). MIT Press.

Worthington, L. V. (1970). The Norwegian Sea as a mediterranean basin. *Deep Sea Research and Oceanographic Abstracts*, *17*(1), 77–84. https://doi.org/10.1016/0011-7471(70)90088-4

Xu, X., Rhines, P. B., Chassignet, E. P., & Schmitz, W. J., Jr. (2015). Spreading of Denmark Strait Overflow water in the western subpolar North Atlantic: Insights from eddy-resolving simulations with a passive tracer. *Journal of Physical Oceanography*, *45*(12), 2913–2932. https://doi.org/10.1175/JPO-D-14-0179.1

Yang, J., & Pratt, L. J. (2014). Some dynamical constraints on upstream pathways of the Denmark Strait Overflow. *Journal of Physical Oceanography*, *44*(12), 3033–3053. https://doi.org/10.1175/JPO-D-13-0227.1

Yashayaev, I. (2007). Hydrographic changes in the Labrador Sea, 1960–2005. *Progress in Oceanography*, *73*(3–4), 242–276. https://doi.org/10.1016/j.pocean.2007.04.015

Zou, S., Lozier, S., Zenk, W., Bower, A., & Johns, W. (2017). Observed and modeled pathways of the Iceland Scotland overflow water in the eastern North Atlantic. *Progress in Oceanography*, *159*, 211–222. https://doi.org/10.1016/j.pocean.2017.10.003

References From the Supporting Information

Frajka-Williams, E., Ansorge, I. J., Baehr, J., Bryden, H. L., Chidichimo, M. P., Cunningham, S. A., et al. (2019). Atlantic meridional overturning circulation: Observed transport and variability. *Frontiers in Marine Science*, *6*, 260. https://doi.org/10.3389/fmars.2019.00260

Frajka-Williams, E., Moat, B. I., Smeed, D. A., Rayner, D., Johns, W. E., Baringer, M. O., et al. (2021). *Atlantic Meridional Overturning Circulation observed by the RAPID-MOCHA-WBTS (RAPID-Meridional Overturning Circulation and Heatflux Array-Western Boundary Time Series) array at 26N from 2004 to 2020 (v2020.1)*. British Oceanographic Data Centre; Natural Environment Research Council. https://doi.org/10.5285/cc1e34b3-3385-662b-e053-6c86abc03444

Kanzow, T., Send, U., Zenk, W., Chave, A. D., & Rhein, M. (2006). Monitoring the integrated deep meridional flow in the tropical North Atlantic: Long-term performance of a geostrophic array. *Deep Sea Research Part I: Oceanographic Research Papers*, *53*(3), 528–546. https://doi.org/10.1016/j.dsr.2005.12.007

Send, U., Lankhorst, M., & Kanzow, T. (2011). Observation of decadal change in the Atlantic Meridional Overturning Circulation using 10 years of continuous transport data. *Geophysical Research Letters*, *38*, L24606.